at a fixed SG concentration, probably because of small difference in the molecular weight of model proteins.

De novo *adipose tissue generation*

Various SGMs immobilized with or without bioactive substances including bFGF, insulin, and IGF-I were prepared at a fixed SG concentration: the SG concentrations used were 20 wt% for bFGF-immobilized SGMs and 30 wt% for insulin- or IGF-I-immobilized SGMs. One hundred milligrams of SGMs was injected into the subcutaneous tissues of Wistar rats. An implantation study was conducted with six different groups as follows. Group I consisted of SGMs immobilized with only bFGF at four different concentrations (μg) per 100 mg of photocured SG, designated Group I (0.01), Group I (0.1), Group I (1), and Group I (10). Group II consisted of SGMs immobilized only with insulin (1 IU per 100 mg of photocured SG), group III consisted of SGMs immobilized only with IGF-I (1 μg per 100 mg of photocured SG), group IV consisted of SGMs immobilized with insulin (1 IU) and IGF-I (1 μg) per 100 mg of photocured SG, and group V consisted of SGMs immobilized with three ingredients (bFGF [1 μg], insulin [1 IU], and IGF-I [1 μg] per 100 mg of photocured SG). Group VI consisted of SGMs immobilized with no bioactive substances.

Effect of bFGF-immobilized microspheres on neovascularization. Figure 4A–E shows macroscopic views of tissues 2 weeks after subcutaneous injection of SGMs with or without bFGF. For Group I, vascularization around the injection site of bFGF-immobilized SGMs became apparent as the amount of bFGF immobilized in SGMs increased. The highest degree of neovascularization was observed for SGMs immobilized with bFGF at a concentration of 1 μg/100 mg of photocured SG, whereas the lowest degree was found for group VI (without bFGF). Figure 4F–J shows results of the histochemical vWF staining of sections of the surrounding tissues in the injection site 2 weeks after the subcutaneous injection of SGMs with or without bFGF. The number of capillaries around the injection site increased as the amount of bFGF immobilized in SGMs increased. The capillary densities of the surrounding tissues 2, 4, and 6 weeks after injection of bFGF-immobilized SGMs, in comparison with those of SGMs without any bioactive substance, are shown in Fig. 5. The highest capillary density was observed for group I (1) 2 weeks after injection, and it was about twice that of the control group (group VI) during the same period; little difference in capillary density was observed 4 and 6 weeks after injection regardless of the group. In comparison with other groups (groups II, III, IV, and V), at 4 weeks postimplantation, there is no significant difference in capillary density between groups, although the mean capillary density of the bioactive substance-immobilized groups, except for the group with the least bFGF, is higher than that of the control (group VI).

Gross observations. Figure 6A–F shows macroscopic views of subcutaneous lesions of groups I (1), II, III, IV, V, and VI, 4 weeks after injection of SGMs immobilized

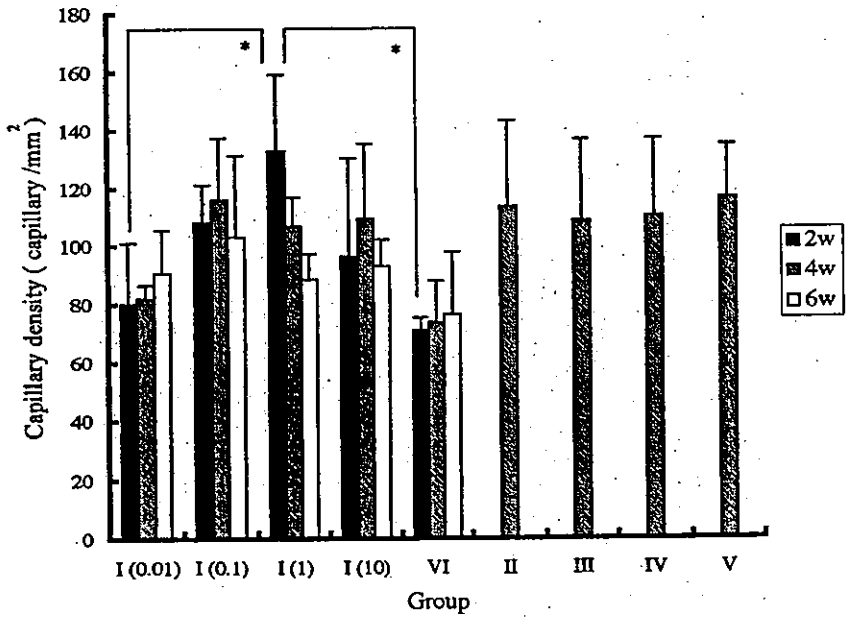

FIG. 5. Capillary density of tissue of the injection site, 2, 4, and 6 weeks after injection of bFGF-immobilized or blank SGMs. Data represent means ± SD. $^*p < 0.05$.

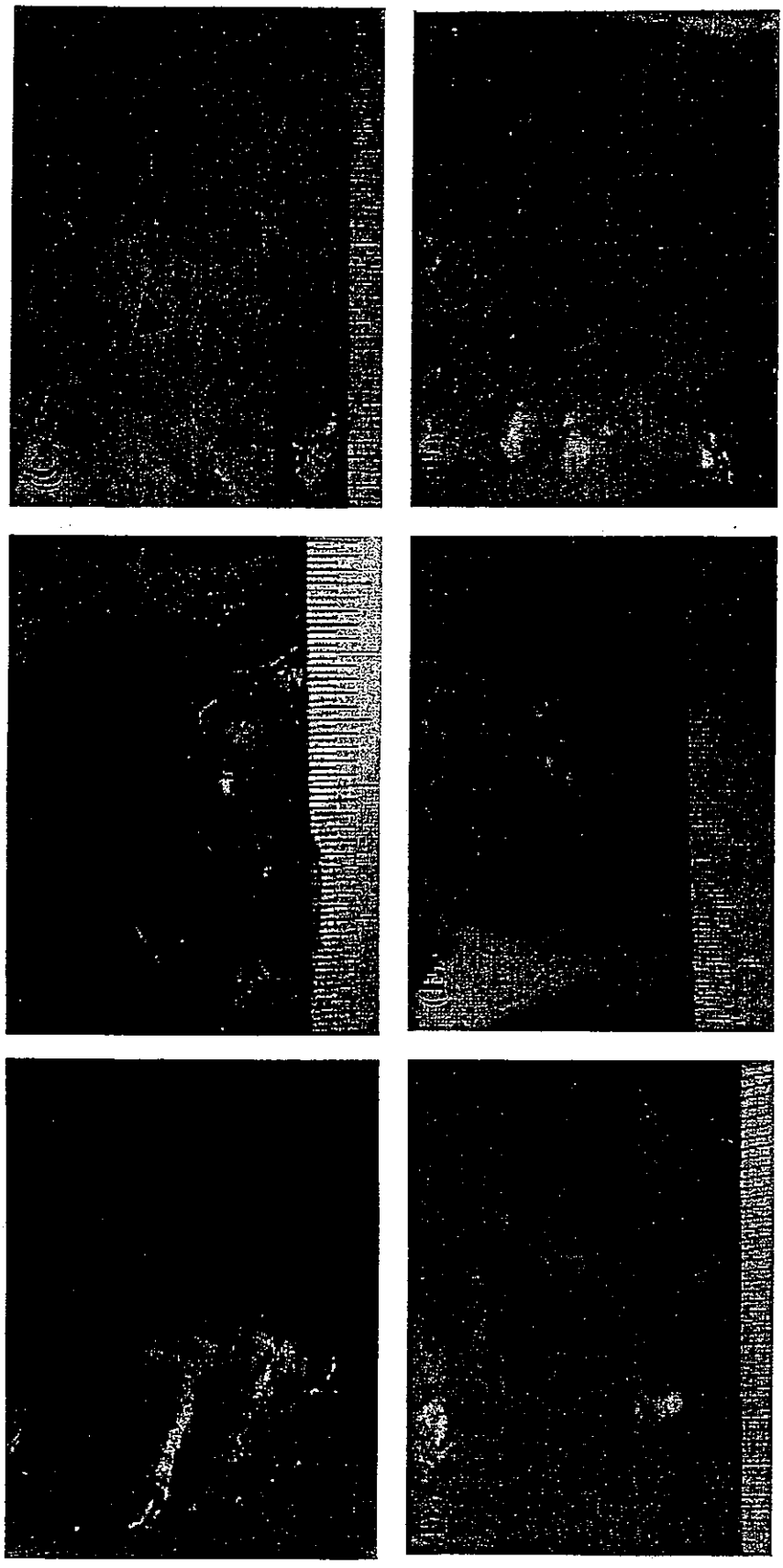

FIG. 6. Tissue appearance of injection site (surrounded by arrows), 4 weeks after injection of SGMs immobilized with various bioactive substances. (A) Group I (1) (SGMs immobilized with 1 μg of bFGF per 100 mg of SG); (B) group II (SGMs immobilized with 1 IU of insulin per 100 mg of SG); (C) group III (SGMs immobilized with 1 μg of IGF-I per 100 mg of SG); (D) group IV (SGMs immobilized with 1 IU of insulin and 1 μg of IGF-I per 100 mg of SG); (E) group V (SGMs immobilized with 1 μg of bFGF, 1 IU of insulin, and 1 μg of IGF-I per 100 mg of SG); (F) group VI (no bioactive substances).

with various bioactive substances. Slightly elevated plaques (approximately 1 × 1 cm^2) were observed at the injection sites of rats in groups I (1), II, III, IV, V, and VI; the most prominent are those of group V (Fig. 6E).

Histology. Figure 7A–L shows the H&E-stained sections of rat subcutaneous lesions of Group I (1), II, III, IV, V, and VI samples 4 weeks after injection of SGMs with or without various bioactive agents. Although partial biodegradation and biosorption occur, residual SGMs remained in all the groups at the injection sites, which were surrounded by tissue composed mainly of collagen fibers and fibroblasts. In groups II–V, masses or clusters of adipocytes were observed between the layers of fibrous tissue. These adipocytes existed in greater number in deeper lesions than in superficial lesions of the residual SGMs. Among these groups, a larger amount of adipose tissue was observed in groups IV and V compared with groups II, III, and VI. In group V, a layer of adipose tissue approximately 1 mm thick was observed adjacent to residual SGMs in deeper lesions. In group VI, however, the injection site was surrounded by a thick layer of connective tissue with few adipocytes interspersed between the layers of fibrous tissue. Sudan IV staining enabled clear visualization of the presence of lipid-containing adipocytes: Sudan IV-positive cells were observed mainly in clusters between the fibrous layers surrounding the residual SGMs, and some cells were also observed among cells that infiltrated residual SGMs (Fig. 8).

Triacylglycerol content. Total lipid at the injection site and surrounding tissue was extracted with chloroform–methanol (2:1, v/v) and triacylglycerol content was determined. In groups IV and V, triacylglycerol content in the surrounding tissues of the injection site were significantly higher than those in groups I (1), III, and VI. Triacylglycerol content in group V was significantly (almost 1.5-fold) higher than that in group IV (Fig. 9).

DISCUSSION

Several studies on the *de novo* formation of adipose tissue by the sustained release of bioactive substances with or without matrixes have been reported. Possible explanations for this adipogenic phenomenon are the migration of endogenous preadipocytes or mesenchymal stem cells into the treated site followed by their pro-

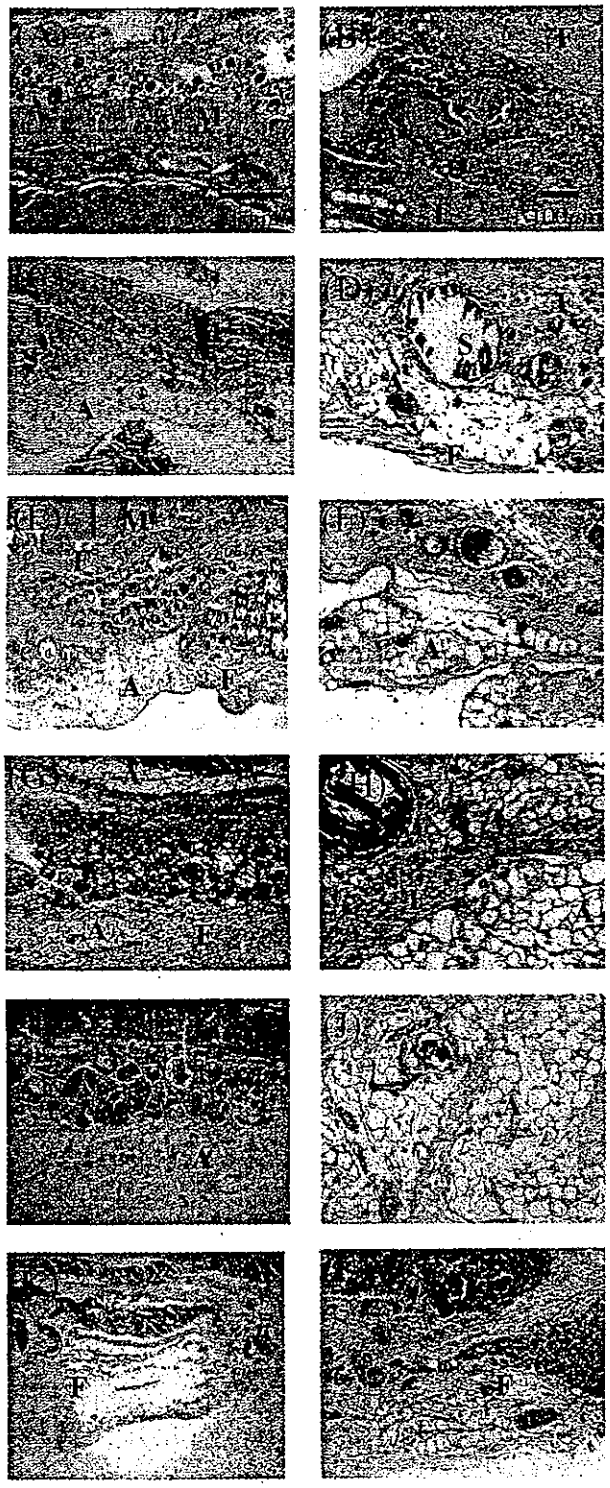

FIG. 7. H&E-stained sections of injection sites, 4 weeks after injection of SGMs immobilized with various bioactive substances. (A and B) Group I (1) (SGMs immobilized with 1 μg of bFGF per 100 mg of SG); (C and D) group II (SGMs immobilized with 1 IU of insulin per 100 mg of SG); (E and F) group III (SGMs immobilized with 1 μg of IGF-I per 100 mg of SG); (G and H) group IV (SGMs immobilized with 1 IU of insulin and 1 μg of IGF-I per 100 mg of SG); (I and J) group V (SGMs immobilized with 1 μg of bFGF, 1 IU of insulin, and 1 μg of IGF-I per 100 mg of SG); (K and L) group VI (no bioactive substances). Original magnifications: (A, C, E, G, and I) ×20; (B, D, F, H, and J) ×100. A, Adipose tissue; F, fibrous layer; M, cutaneous muscle of the trunk, S, residual SGMs.

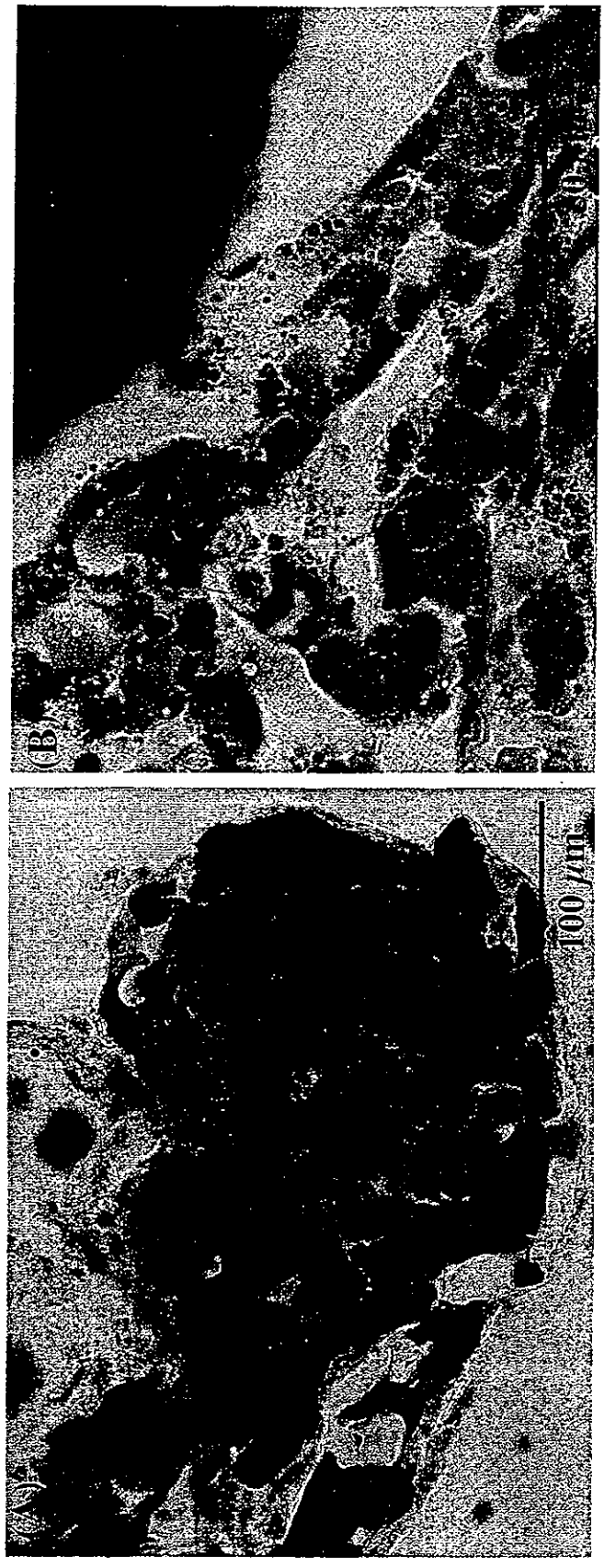

FIG. 8. Representative Sudan IV-stained sections of lipid-containing adipocytes in group V. (A) Adipocytes were observed mainly in clusters between the fibrous layers surrounding the injection site of bioactive substance-immobilized SGMs. (B). Some Sudan IV-positive cells were also observed among cells that infiltrated around residual SGMs.

liferation and differentiation to mature adipocytes.[11–14] Various hormones, cytokines, and growth factors modulate adipocyte differentiation. Among them, insulin and IGF-I separately stimulate adipocyte proliferation and the adipogenic differentiation of nonadipocyte cells to mature adipocytes.[19,20] Angiogenic factors (e.g., bFGF) play a critical role in neovascularization for blood supply and oxygenation, and for recruitment and proliferation of preadipocytes.[11–13,21] For example, the amount of newly formed adipose tissue increased with an increase in the concentration of bFGF, which was immobilized in Matrigel.[11] On the other hand, there appeared to be an optimal dose of bFGF immobilized in gelatin microspheres for adipose tissue formation.[12]

The major issue in adipose tissue regeneration technology is how to accelerate adipose tissue formation and how to regenerate a large amount of adipose tissue in the site of soft tissue defects. One possible means of accelerating adipose tissue formation is to realize the concerted actions of neovascularization and accumulation of preadipocytes, which are driven by the gradual release of angiogenic factors (e.g., bFGF),[11,12,22,23] which should operate in the early phase of implantation, followed by the differentiation of preadipocytes to mature adipocytes as induced by the sustained release of adipogenic factors[14–16] in the later stage. If these two different biological events synchronously or sequentially occur, adipose tissue formation would be accelerated. On the basis of the above-mentioned working principle, we attempted to devise a local drug delivery system that simultaneously releases these biological substances with different release rates. To this end, microspheres made of photocurable, styrenated gelatin were employed as a drug-immobilizing and -releasing matrix.[17] The study on the release characteristics of rhodamine–lactalbumin and FITC–insulin from gel into PBS revealed that the release rate is dependent on SG concentration, independent of the type of model drugs used within the range of the molecular weight tested (approximately 6×10^3–1.4×10^4) (Fig. 3A and B). The release rate was highest for the gel prepared with the lowest gelatin concentration (20%), which was employed for immobilization of bFGF for the rapid release of an angiogenic factor. Denser SGMs, prepared at 30% gelatin concentration, were employed for immobilization of insulin and IGF-I, aiming at a slower release of adipogenic factors than the former version. These microspheres, which were not mechanically fragile, withstood the mechanical stress applied during injection and implantation.

However, it is of importance to verify and discuss how the *in vitro* releasing profile of a protein can correlate with the *in vivo* releasing profile. We did not conduct any such experiment in this study. It is noteworthy to cite briefly a series of studies by Tabata *et al.*[24,25] They used glutaraldehyde-cross-linked "acidic" gelatin (isoelectric point [IEP], 5.0) as a drug carrier, in which bFGF is sorbed from an aqueous solution. *In vitro* releasing from cross-linked gelatin was inhibited because of ionic interaction between bFGF (IEP, 9.6) and acidic gelatin, except for the burst release within the first day of immersion into buffer solution. However, in animal experiments, radioisotope-labeled bFGF was continuously released with implantation time because of proteolytic biodegradation of gelatin. This indicates that *in vitro* releasing characteristics did not reflect *in vivo* releasing characteristics. This must also have occurred in this experiment. Although the IEP of gelatin used in this study was not determined, the *in vitro* releasing profile in Fig. 3A must be due to the

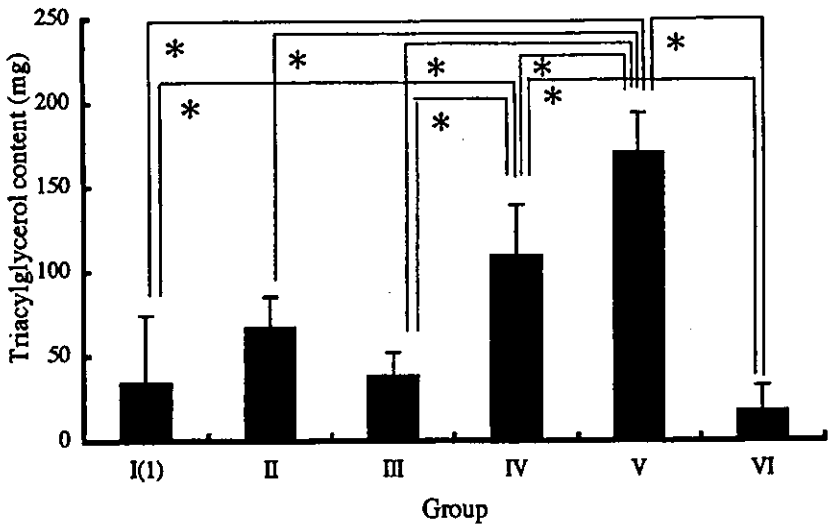

FIG. 9. Total lipid was extracted from SGM injection site tissue and triacylglycerol content was measured as described in Materials and Methods. Data represent means ± SD. $^*p < 0.05$.

combined contribution of size effects of the protein used and some ionic interaction between proteins and gelatin under no proteolytic biodegradation, as mentioned above. Therefore, it is highly anticipated that such a releasing profile does not necessarily correlate with the *in vivo* releasing profile. If biodegradation is a major determinant for release, the time course of released bioactive substances must depend on the degree of photocuring and gelatin concentration, which are principal determinants for biodegradiation as previously reported by us.[17]

A high angiogenesis potential of bFGF-immobilized SGMs was noted (Fig. 4F–J). The capillary densities at the sites treated with bFGF-immobilized SGMs were higher compared with those at the sites treated with SGMs without bFGF (Fig. 5). The capillary density appears to be dependent on bFGF concentration as well as implantation period. At the earlier stage after injection (2 weeks), the highest capillary density was observed at the site treated with group I (1) (1 μg of bFGF immobilized per 100 mg of SG): the capillary density was almost 2-fold higher than that of the site treated with SGMs without bFGF. However, such dependency appears to diminish at a prolonged period after injection (6 weeks). The observed tendency is in good agreement with those previously reported.[26,27] These findings suggest that bFGF released from SGMs induces rapid neovascularization at an early stage after injection.

The study on subcutaneous injection of SGMs immobilized with either an adipogenic factor or combined angiogenic and adipogenic factors clearly showed the possibility of adipose tissue formation (Figs. 7 and 8). Among the groups studied, the largest amount of adipose tissue was observed for the group that received a mixture of three different SGMs, each of which was immobilized with respective bioactive substances (group V). Triacylglycerol content at the site of SGM injection in group V was about 1.5-fold higher than in the group that received a combination of SGMs immobilized with insulin and IGF-I (group IV). This *de novo* adipogenesis is achieved by creating a microenvironment for recruiting endogenous preadipocytes, which subsequently undergo proliferation and differentiation. A single injection of two types of SGMs with two different drug release rates enabled induction of the two-step biological events.

The advantageous features of photocurable gelatin as a drug-immobilized matrix include (1) a controlled degree of cross-linking, which can achieved by the degree of derivatized styrene group in a gelatin molecule, the concentration of styrenated gelatin, and the photocuring time, which is a determinant for the drug-releasing rate as well as the biodegradation rate, and (2) simultaneous photocuring of SG and highly effective immobilization of protein (the amount of protein immobilized can be determined from the formulation during microsphere preparation, due to expected high immobilization efficacy). Water-soluble SG and protein, both of which are not soluble in paraffin, should exist in water phase during microsphere preparation. Therefore, high immobilization efficacy is expected in principle. As for biological activity in immobilized proteins, minor loss of biological activity during photocuring process may not be ruled out. SGMs did not induce substantial damage at cell and tissue levels after the injection of SGMs without any bioactive substances into rat subcutaneous tissue (Fig. 7I and J). Therefore, SGMs can serve as a nontoxic local drug delivery system with easy control of drug immobilization and drug release characteristics.[17]

Although the application of this two-step method for pharmacologically stimulated *de novo* adipose tissue formation is effective, further improvements are required before clinical application of this system. One is to sufficiently increase the amount of newly formed adipose tissue to meet the requirement of soft tissue augmentation and the other is to reduce local fibrosis around injection sites, which occurs with *de novo* adipogenesis. Further studies need to be conducted not only to minimize side effects, but also to maximize the amount of newly formed adipose tissue for soft tissue augmentation. These include optimization of the amount of angiogenic and adipogenic factor, drug release rate, and local inflammation control.

ACKNOWLEDGMENTS

This study was financially supported in part by the Promotion of Fundamental Studies in Health Science of the Organization for Pharmaceutical Safety and Research (OPSR), grant 97-15, and in part by a Grant-in-Aid for Scientific Research (A2-12358017 and B2-12470277) and by a Grant-in-Aid for the Creation of Innovations through Business-Academic-Public Sector Cooperation from the MEXT of Japan. The authors thank Mr. Takaaki Kanemaru (Morphology Core, Graduate School of Medical Sciences, Kyushu University) for SEM observation.

REFERENCES

1. Katz, A.J., Llull, R., Hedrick, M.H., and Futrell, J.W. Emerging approaches to the tissue engineering of fat. Clin. Plast. Surg. **26**, 587, 1999.
2. Billings, E., Jr., and May, J.W., Jr. Historical review and present status of free fat graft autotransplantation in plastic and reconstructive surgery. Plast. Reconstr. Surg. **83**, 368, 1989.
3. Chajchir, A. Fat injection: Long-term follow-up. Aesthetic Plast. Surg. **20**, 291, 1996.
4. Kononas, T.C., Bucky, L.P., Hurley, C., and May, J.W., Jr. The fate of suctioned and surgically removed fat after reimplantation for soft-tissue augmentation: A volumetric and

histologic study in the rabbit. Plast. Reconstr. Surg. **91,** 763, 1993.
5. Green, H., and Kehinde, O. Formation of normally differentiated subcutaneous fat pads by an established preadipose cell line. J. Cell. Physiol. **101,** 169, 1979.
6. Patrick, C.W., Jr., Chauvin, P.B., Hobley, J., and Reece, G.P. Preadipocyte seeded PLGA scaffolds for adipose tissue engineering. Tissue Eng. **5,** 139, 1999.
7. Schoeller, T., Lille, S., Wechselberger, G., Otto, A., Mowlawi, A., and Piza-Katzer, H. Histomorphologic and volumetric analysis of implanted autologous preadipocyte cultures suspended in fibrin glue: A potential new source for tissue augmentation. Aesthetic Plast. Surg. **25,** 57, 2001.
8. von Heimburg, D., Zachariah, S., Heschel, I., Kuhling, H., Schoof, H., Hafemann, B., and Pallua, N. Human preadipocytes seeded on freeze-dried collagen scaffolds investigated in vitro and in vivo. Biomaterials **22,** 429, 2001.
9. Patrick, C.W., Jr., Zheng, B., Johnston, C., and Reece, G.P. Long-term implantation of preadipocyte-seeded PLGA scaffolds. Tissue Eng. **8,** 283, 2002.
10. Halberstadt, C., Austin, C., Rowley, J., Culberson, C., Loebsack, A., Wyatt, S., Coleman, S., Blacksten, L., Burg, K., Mooney, D., and Holder, W., Jr. A hydrogel material for plastic and reconstructive applications injected into the subcutaneous space of a sheep. Tissue Eng. **8,** 309, 2002.
11. Kawaguchi, N., Toriyama, K., Nicodemou-Lena, E., Inou, K., Torii, S., and Kitagawa, Y. *De novo* adipogenesis in mice at the site of injection of basement membrane and basic fibroblast growth factor. Proc. Natl. Acad. Sci. U.S.A. **95,** 1062, 1998.
12. Tabata, Y., Miyao, M., Inamoto, T., Ishii, T., Hirano, Y., Yamaoki, Y., and Ikada, Y. De novo formation of adipose tissue by controlled release of basic fibroblast growth factor. Tissue Eng. **6,** 279, 2000.
13. Kimura, Y., Ozeki, M., Inamoto, T., and Tabata, Y. Time course of de novo adipogenesis in matrigel by gelatin microspheres incorporating basic fibroblast growth factor. Tissue Eng. **8,** 603, 2002.
14. Yuksel, E., Weinfeld, A.B., Cleek, R., Waugh, J.M., Jensen, J., Boutros, S., Shenaq, S.M., and Spira, M. De novo adipose tissue generation through long-term, local delivery of insulin and insulin-like growth factor-1 by PLGA/PEG microspheres in an in vivo rat model: A novel concept and capability. Plast. Reconstr. Surg. **105,** 1721, 2000.
15. Yuksel, E., Weinfeld, A.B., Cleek, R., Jensen, J., Wamsley, S., Waugh, J.M., Spira, M., and Shenaq, S. Augmentation of adipofascial flaps using the long-term local delivery of insulin and insulin-like growth factor-1. Plast. Reconstr. Surg. **106,** 373, 2000.
16. Yuksel, E., Weinfeld, A.B., Cleek, R., Wamsley, S., Jensen, J., Boutros, S., Waugh, J.M., Shenaq, S.M., and Spira, M. Increased free fat-graft survival with the long-term, local delivery of insulin, insulin-like growth factor-I, and basic fibroblast growth factor by PLGA/PEG microspheres. Plast. Reconstr. Surg. **105,** 1712, 2000.
17. Okino, H., Nakayama, Y., Tanaka, M., and Matsuda, T. In situ hydrogelation of photocurable gelatin and drug release. J. Biomed. Mater. Res. **59,** 233, 2002.
18. Matsuda, T., and Magoshi, T. Preparation of vinylated polysaccharides and photofabrication of tubular scaffolds as potential use in tissue engineering. Biomacromolecules **3,** 942, 2002.
19. Caplan, A.I. The mesengenic process. Clin. Plast. Surg. **21,** 429, 1994.
20. Gregoire, F.M., Smas, C.M., and Sul, H.S. Understanding adipocyte differentiation. Physiol. Rev. **78,** 783, 1998.
21. Eppley, B., Sidner, R., Platis, J., and Sadove, M. Bioactivation of free-fat transfers: A potential new approach to improving graft survival. Plast. Reconstr. Surg. **90,** 1022, 1992.
22. Rupnick, M.A., Panigrahy, D., Zhang, C.Y., Dallabrida, S.M., Lowell, B.B., Langer, R., and Folkman, M.J. Adipose tissue mass can be regulated through the vasculature. Proc. Natl. Acad. Sci. U.S.A. **99,** 10730, 2002.
23. Babensee, J.E., McIntire, L.V., and Mikos, A.G. Growth factor delivery for tissue engineering. Pharm. Res. **17,** 497, 2000.
24. Tabata, Y., and Ikada, Y. Protein release from gelatin matrices. Adv. Drug Deliv. Rev. **31,** 287, 1998.
25. Yamamoto, M., Ikada, Y., and Tabata, Y. Controlled release of growth factors based on biodegradation of gelatin hydrogel. J. Biomater. Sci. Polym. Ed. **12,** 77, 2001.
26. Tabata, Y., Hijikata, S., Muniruzzaman, M., and Ikada, Y. Neovascularization effect of biodegradable gelatin microspheres incorporation basic fibroblast growth factor. J. Biomater. Sci. Polymer Ed. **10,** 79, 1999.
27. Tanihara, M., Suzuki, Y., Yamamoto, E., Noguchi, A., and Mizushima, Y. Sustained release of basic fibroblast growth factor and angiogenesis in a novel covalently crosslinked gel of heparin and alginate. J. Biomed. Mater. Res. **56,** 216, 2001.

Address reprint requests to:
Takehisa Matsuda, Ph.D.
Department of Biomedical Engineering
Graduate School of Medicine
Kyushu University
3-1-1 Maidashi, Higashiku
Fukuoka 812-8582, Japan

E-mail: matsuda@med.kyushu-u.ac.jp

Available online at www.sciencedirect.com
SCIENCE DIRECT®
Biomaterials 25 (2004) 5867–5873
Biomaterials
www.elsevier.com/locate/biomaterials

In situ-formed, tissue-adhesive co-gel composed of styrenated gelatin and styrenated antibody: potential use for local anti-cytokine antibody therapy on surgically resected tissues

Tatsuya Manabe[a,b], Hidenobu Okino[a,b], Masao Tanaka[b], Takehisa Matsuda[a,*]

[a] *Divisions of Biomedical Engineering, Graduate School of Medicine, Kyushu University, 3-1-1 Maidashi, Fukuoka City, Fukuoka 812-8582, Japan*
[b] *Division of Surgery and Oncology, Graduate School of Medicine, Kyushu University, 3-1-1 Maidashi, Fukuoka 812-8582, Japan*

Received 24 October 2003; accepted 20 January 2004

Abstract

Styrenated antibody (ST-Ab) and styrenated gelatin (ST-gelatin) were prepared by condensation reaction of antibody or gelatin with 4-vinylbenzoic acid, respectively. The affinity loss of ST-Ab to its antigen was minimal. ST-Ab and ST-gelatin were copolymerized with by visible-light irradiation in the presence of a water-soluble camphorquinone as a photoinitiator to produce a tissue-adhesive, in situ-formed co-gel of ST-gelatin and ST-Ab. The amount of non-reacted ST-Ab released from the co-gel of ST-gelatin and ST-Ab into the medium was minimal. The confocal laser scanning microscopy observation showed that local accumulation of rhodamine-labeled bovine serum albumin (BSA) as a model antigen was noticed in the surface-to-subsurface region of the co-gel of ST-gelatin and anti-BSA ST-Ab, indicating that the gel prevented the permeation of BSA into the gel. In invasion double chamber assay using anti-hepatocyte growth factor (HGF) antibody, the co-gel prevented HGF-dependent invasion of pancreatic cancer cells. The discussion was made for potential application of an in situ-formed tissue-adhesive co-gel of ST-gelatin and ST-Ab, developed in this study, as a cytokine-barrier on a surgically resected tissue where cancer cells might still remain after resection of cancerous tissue.

Keywords: Photoreactive gelatin; Photoreactive antibody; Local antibody therapy

1. Introduction

Various therapeutic approaches toward the cure from cancer, which is one of the most incurable diseases, have been explored and attempted. As for biomaterials-based therapeutic procedures, systemic administration of micelle-type drug and polymer-bound controlled drug delivery system based on biodegradable matrices have been experimentally explored and their therapeutic effectiveness have been proven [1–4]. However, surgical resection is still the first and most effective therapeutic choice when the malignant tissue is localized without distant metastases. As for pancreatic cancer, resection is the only curative modality, but the survival rate of resected patients is still very low [5,6]. The major reason is that pancreatic cancer cells often remain in the retroperitoneal space after surgery, and subsequently induce local recurrence at a high incidence (50–80%) [7]. Therefore, new therapeutic modalities to prevent local recurrence after surgery have been awaited.

Such a malignant behavior is usually accelerated by various cytokines related to inflammations and tissue regenerations after surgery, such as hepatocyte growth factor (HGF), epidermal growth factor (EGF), basic fibroblast growth factor (bFGF), and transforming growth factor-β (TGF-β) [8]. Among them, HGF, which is known to act as multipotent tissue-regenerating and tumor-progressing factor, affects most potently the invasiveness of carcinoma cells [9–17]. HGF is produced and accumulated in the intraperitoneal space after abdominal operation, resulting in an activation of the malignant potentials of remnant cancer cells (Fig. 1A) [17–21].

Recently, monoclonal antibody-based molecular targeting therapy aimed at cytokine deactivation has been developed in cancer treatment [22]. For example, an

*Corresponding author. Tel.: +81-92-642-6210; fax: 81-92-642-6212.
E-mail address: matsuda@med.kyushu-u.ac.jp (T. Matsuda).

0142-9612/$ - see front matter © 2004 Elsevier Ltd. All rights reserved.
doi:10.1016/j.biomaterials.2004.01.036

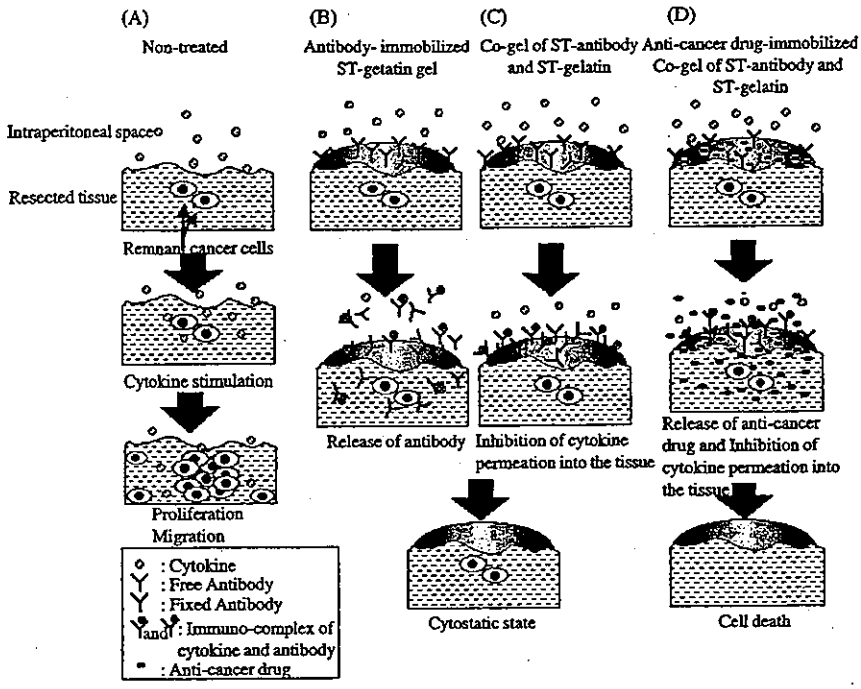

Fig. 1. Schematic of the strategy for local anti-cytokine antibody therapy using in situ photocured gel. (A) Various cytokines produced and accumulated in the intraperitoneal space during wound healing after abdominal surgery and affect remnant cancer cells in surgically resected tissues. (B) Non-treated antibody-immobilized ST-gelatin gel on resected tissues. Antibodies neutralize cytokines in and out of a gel and prevent the effect of cytokines on remnant cancer cells. The antibody-antigen complexes also penetrate into resected tissues. (C) The co-gel of ST-gelatin and anti-cytokine ST-Ab on resected tissues. Antibodies fixed in a gel neutralize cytokines, which permeated into a gel, thereby preventing the permeation and penetration of cytokines into resected tissues. (D) Anti-cancer drug-immobilized co-gel of ST-Ab and ST-gelatin on resected tissue. Cytokine permeation into the tissue was prevented, and anti-cancer drug released from the gel induced cell death.

anti-EGF receptor monoclonal antibody or an anti-vascular endothelial growth factor (VEGF) monoclonal antibody has been systemically administered to reduce the growth of cancerous tissues [23–25]. However, in the early period after surgery, when prompt tissue regeneration accelerated by cytokines is necessary at the resected tissues, particularly the anastomotic site, systemically administered molecular-targeted antibody might induce the inhibition of wound healing. Thus, local antibody delivery must have some advantages because locally delivered antibody could not affect distant site compared with systemic administration.

Previously we have proposed a local delivery system of drugs, proteins or gene-encoding adenoviral vectors using in situ photocured gelatin gel, which is based on styrenated gelatin (ST-gelatin) [26–28]. ST-gelatin is in situ photopolymerized by visible-light irradiation in the presence of a water-soluble camphorquinone as a photoinitiator to produce a gel, which adheres well on surgically resected tissues. In this article, styrenated antibody (ST-Ab) was prepared to copolymerize with ST-gelatin, producing a tissue-adhesive, gelatinous co-gel of ST-gelatin and ST-Ab (Fig. 2A). When the co-gel of ST-gelatin and anti-cytokine ST-Ab is produced on surgically resected tissue where cancer cells might remain, it was anticipated to work well as a cytokine-barrier (Fig. 1C). Herein we present the preparation of ST-Ab and a co-gel of ST-gelatin and ST-Ab, and its in vitro performance, and discuss potential use in clinical settings and new local anti-cytokine therapy using the antibody-bound co-gel.

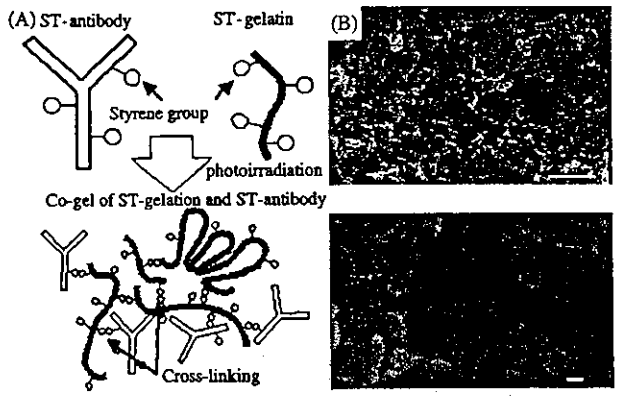

Fig. 2. (A) ST-gelatin (MW 95,000), ST-Ab (MW 150,000), and their polymerization. The average numbers of styrene groups derivatized into gelatin and antibody molecule were approximately 27.3 and 5.1, respectively. Photogelation mechanism by formation of inter- and intramolecular polymerization of ST-gelatin and ST-Ab. (B) SEM observation showed the network mesh and multiple micropores of the surface structure of the co-gel. Bar: 1 μm in upper figure; 100 nm in lower figure.

2. Methods

2.1. Materials

The reagents used and their suppliers were as follows: bovine serum albumin (BSA, MW 6.6×10^4 g/mol) and gelatin (from bovine, MW 9.5×10^4 g/mol) from Wako Pure Chemical Ind., Inc. (Osaka, Japan); 4-vinylbenzoic acid from Tokyo Chemicals Inc., Co., Ltd. (Tokyo, Japan); 1-ethyl-3-(3-dimethylaminopropyl)carbodiimide hydrochloride (WSC) from Dojindo Laboratory (Kumamoto, Japan); rhodamine-conjugated BSA from Sigma-Aldrich Inc. (St. Louis, MO); anti-BSA rabbit IgG antibody from Rockland Inc. (Gilbertsville, PA); phosphate-buffered saline solution (PBS, pH 7.4) from Nissui Pharmaceutical Co. Ltd. (Tokyo, Japan); and anti-human HGF antibody from Techne Co. (Minneapolis, MN). (1*S*)-7,7-Dimethyl-2,3-dioxobicyclo[2.2.1]-heptane-1-carboxylic acid (carboxylated camphorquinone, CQ) was prepared according to the method described previously [26]. The preparation of ST-gelatin was already described in detail in our previous paper [26–29]. The average number of styrene groups derivatized into a gelatin molecule, determined from its absorbance (4-vinylbenzoic acid at 268 nm) as described previously, was 27.3 per molecule.

2.2. Styrenated antibody

The derivatization of a styrene group to IgG antibody molecules was carried out by similar method to ST-gelatin treatment [26–29]. Briefly, an anti-BSA ST-Ab was prepared as follows (for anti-HGF antibody, the reaction feed was scaled down): 4-Vinylbenzoic acid (5.9 mg, 3.98×10^{-5} mol) was dissolved in 15 ml of 0.1 N sodium hydroxide and then neutralized to pH 7.5 with hydrochloric acid. After the addition of WSC (246.7 mg, 1.28×10^{-3} mol), the reaction solution was stirred at 4°C for 30 min and mixed with the anti-BSA antibody (10 mg, 6.7×10^{-8} mol) dissolved in 15 ml of PBS. The reaction mixture was stirred at 4°C for 1 h, dialyzed, and lyophilized to yield a white powder (ST-Ab). The average number of styrene groups derivatized into the antibody molecule, determined from its absorbance, was approximately 5.1 for both anti-BSA and anti-HGF ST-Ab.

The affinity of anti-BSA ST-Ab to its antigen was determined by enzyme-linked immunosorbent assay (ELISA) and compared with that of the non-treated anti-BSA antibody. Using a 96-well microtiter plate (Corning Inc., NY), coated with BSA at various concentrations (50, 100, and 500 ng/50 μl), blocked with 2% sheep serum (Sigma-Aldrich, Inc.) and subsequently washed 3 times with PBS, 60 μl of either non-treated anti-BSA antibody solution (10 μg/ml) or anti-BSA ST-Ab solution (10 μg/ml) was added to the well and the plate was incubated for 1 h at room temperature. After washing five times with PBS, 100 μl of 1:10,000 alkaline phosphatase-conjugated anti-rabbit IgG goat IgG (Sigma-Aldrich, Inc.) was added to the well and the plate was again incubated for 1 h at room temperature. Then, 100 μl of pNPP substrate (4-nitrophenyl phosphate disodium salt solution, Sigma-Aldrich, Inc.) was added and color development, as a quantitative measure of the level of antigen–antibody complex based on coloration, was monitored at 405 nm using a spectrophotometer (Bio-Rad Laboratories, Inc., Hercules, CA).

2.3. Preparation of co-gel of ST-gelatin and ST-Ab and scanning electron microscopic observation

ST-gelatin solution (30 wt%) was used in this study because its viscosity and adhesive strength were optimum [26]. A typical co-gel of ST-gelatin and ST-Ab was prepared as follows. The solution containing 700 μl of PBS, 300 mg of ST-gelatin (30 wt% based on the total gel weight), 2 mg of ST-Ab (0.2 wt% based on the total gel weight), and 0.15 mg of CQ (0.05 wt% based on the ST-gelatin weight) were stirred thoroughly with a high-speed rotating shaker (MX-201, Thinky Co. Ltd., Tokyo, Japan). Then, the solution was photogelled upon visible-light irradiation using an 80-W halogen lamp (Tokuso Power Lite, Tokuyama Co. Ltd., Tokuyama, Japan) (Fig. 2A). Light intensity was 1.3×10^6 lx as measured with a photometer (ANA-F11, Tokyo Kohden Co. Ltd., Tokyo, Japan). The co-gel was fixed in 2% glutaraldehyde (Electron Microscopy Sciences, Morris Road, Washington, PA) for 1 h and then postfixed in 1% osmium tetroxide (Chiyoda Junyaku, Tokyo, Japan) for 1 h, and subsequently dehydrated with a graded series of ethanol, sputter-coated with platinum and evaluated by scanning electron microscopy (SEM) (JEOL, JSM-840A, Tokyo, Japan).

2.4. Release of non-reacted ST-Ab and permeation of antigen

To assess the reaction of copolymerization between ST-gelatin and ST-Ab, the amount of antibody released from the co-gel was examined compared with non-treated antibody-immobilized gel using western blot analysis. Disk-type photocured gels (150 mg; 78.5 mm^2), which were composed of ST-gelatin (30 wt%) in Group 1, ST-gelatin (30 wt%) and non-treated anti-BSA rabbit antibody (0.2 wt%) in Group 2, and ST-gelatin (30 wt%) and anti-BSA rabbit ST-Ab (0.2 wt%) in Group 3, were immersed in 1 ml of PBS for 24 h, and then the supernatants were collected and subjected to western blot analysis. The proteins released from the gels were fractionated by 10% sodium dodecyl sulfate-polyacrylamide gel electrophoresis and transferred to a polyvinylidene difluoride membrane (Millipore,

Bedford, MA). The membrane was incubated with 1: 200 FITC-conjugated anti-rabbit IgG antibody and then photographed using a Molecular Imager FX (Bio-Rad Laboratories Inc.).

To determine the inhibitory effect of the co-gel of ST-gelatin and anti-BSA ST-Ab for permeation of the antigen, three different disk-shaped mixed gels were immersed in 5 ml of 26.4 μg/ml rhodamine-conjugated BSA solution. After 24, 36, and 60 h of incubation at 37°C, the maximum transverse cryostat sections of the gels were prepared with a microslicer (CM 1850, Leica, Nussloch, Germany). The sections were observed and quantitatively determined from the depth profile of fluorescence intensity from the surface using a confocal laser scanning microscopy (CLSM, 595 nm excitation, Bio-Rad Laboratories Inc.).

2.5. Invasion assay

To assess the inhibitory effect of the co-gel as a cytokine-barrier, HGF-dependent invasion of tumor cells was measured with the co-gel of ST-gelatin and anti-HGF ST-Ab using a 24-well Matrigel invasion double chamber (Becton Dickinson, Bedford, MA) (Fig. 6A) [13–17]. Pancreatic cancer cells (SUIT-2) [30], generously donated by Dr. H. Iguchi, were cultured and then suspended in DMEM containing 2% fetal bovine serum (FBS) at 37°C in 5% CO_2. The suspension was added to the inner cup of the Matrigel invasion chamber at a density of 5×10^4 cells/cup. After 6 h of cultivation, the medium was removed, and 10 mg each of the photocured gelatin solutions [Group 1, ST-gelatin (30 wt%) only; Group 2, ST-gelatin (30 wt%) and non-treated anti-HGF antibody (0.2 wt%); or Group 3, ST-gelatin (30 wt%) and anti-HGF ST-Ab (0.2 wt%)] was overlayered on the seeded cells and subsequently photogelled. In Group 0, a gel was not used. Then, 500 μl of DMEM with or without 10 or 50 ng/ml human HGF was added to the inner cup. DMEM (750 μl) containing 2% FBS was added to the outer well and the inner cup was inserted into the outer well. After 24 h of cultivation, the pancreatic cancer cells, that degraded the Matrigel and migrated through 8-μm pores of the membrane at the bottom of the inner cup to the opposite side of the membrane, were counted after hematoxylin and eosin staining. Five microscopic fields (× 200) were randomly selected for cell counting.

3. Results

3.1. Co-gel of ST-gelatin and ST-Ab

The anti-BSA ST-Ab and ST-gelatin were prepared using 4-vinylbenzoic acid according to our previous method [26–29]. As shown in Fig. 3, the degree of the affinity of anti-BSA ST-Ab to BSA, as determined by ELISA, was found to be almost the same as non-ST-Ab. To determine whether the anti-BSA ST-Ab was copolymerized with ST-gelatin, the anti-BSA ST-Ab released from the co-gel into PBS was assayed by western blot analysis using three different disk-type gels [Group 1, only ST-gelatin gel (30 wt%); Group 2, ST-gelatin gel (30 wt%) mixed with non-treated anti-BSA rabbit antibody (0.2 wt%); and Group 3, co-gel of ST-gelatin (30 wt%) and anti-BSA rabbit ST-Ab (0.2 wt%)]. As shown in Fig. 4, the amount of heavy

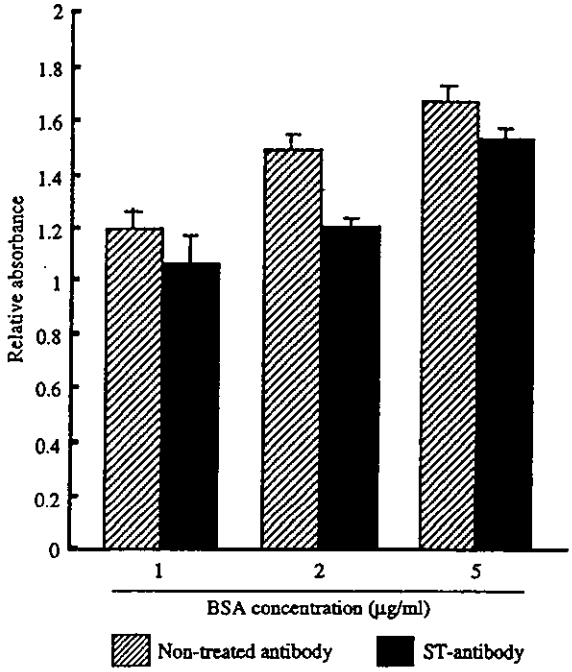

Fig. 3. The affinity of anti-BSA ST-Ab to its antigen was determined by ELISA and compared with that of non-treated anti-BSA antibody ($n = 3$). The affinity of anti-BSA ST-Ab to BSA was observed to be restored.

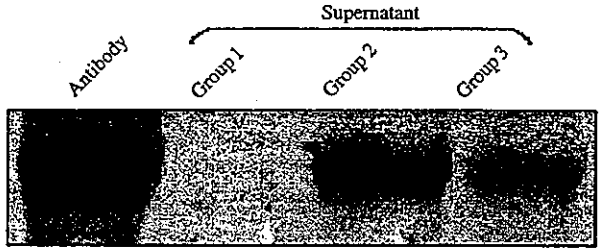

Fig. 4. Amount of ST-Ab released from the co-gel of ST-gelatin and ST-Ab. Disk-type photocured gelatin gels composed of ST-gelatin (Group 1), ST-gelatin and non-treated anti-BSA antibody (Group 2), and ST-gelatin and anti-BSA ST-Ab (Group 3) were immersed in PBS for 24 h, and then the supernatants were collected and subjected to western blot analysis. The amount of heavy chain of the antibody was much larger in Group 2 than in Group 3. This result suggests that a minimal amount of non-reacted ST-Ab is released, indicating that the majority of ST-Ab copolymerizes in a gel.

chain of IgG antibody released from the co-gel was much larger in Group 2 where non-treated anti-BSA antibody was simply mixed in a ST-gelatin gel than that in Group 3. This result indicates that the amount of ST-Ab released from a co-gel is reduced, indicating that anti-BSA ST-Ab is copolymerized with ST-gelatin to form a copolymerized gel. SEM observation revealed that the co-gel of ST-gelatin and ST-Ab was found to form gelatinous network meshes, which was composed of approximately one-hundred-nanometer-scale fibers, globules, and open-structured interconnecting microvoids or channels at the surface and interior regions (Fig. 2B).

3.2. Permeation of antigen into gels

To determine whether the copolymerized gel composed of anti-BSA ST-Ab and ST-gelatin inhibits or retards BSA permeation, rhodamine-conjugated BSA solution was pored over the disks, and time-development cross-sectional permeation characteristics were visually and quantitatively monitored by a CLSM. As shown in Fig. 5A, irrespective of the groups, BSA tended to localize on the surface region of the gels at an early period of immersion, followed by its gradual permeation into the interior of the gels and into deeper regions with time. However, the permeation in Group 3 (the co-gel of ST-Ab and ST-gelatin) was the slowest among three groups, and the co-gel in Group 3 appeared to trap a dye-conjugated BSA. On the other hand, there was no significant difference in permeation characteristics between Groups 1 and 2. After a long time, dye-conjugated BSA homogeneously distributed all over the gel. This was quantitatively determined from the depth profile of fluorescence intensity from the surface, as shown in Fig. 5B. In Group 3, permeated BSA molecules were limited in the surface region after a 36-h permeation period and were still mostly localized and limited in surface-to-subsurface regions even after a 60-h permeation period, as compared with the other two groups in which there was high accumulation in surface-to-subsurface regions and homogeneous distribution in deeper regions. This characteristic is derived from a concentration-dependent phenomenon; at a high BSA concentration relative to the immobilized antibody concentration, the majority of non-complexed BSA permeated through the gel, and at a low BSA concentration, immuno-complex is formed and localized at the surface region (data not shown). This means that a sufficient amount of antibody relative to the permeating antigen is necessary to prevent permeation of its antigen into a tissue.

3.3. Invasion assay

To determine whether the co-gel of ST-gelatin and anti-HGF ST-Ab inhibits HGF permeation, an invasion assay using pancreatic cancer cells (SUIT-2) was performed with 10 mg each of the photocured gels [Group 1, gel prepared from ST-gelatin (30 wt%); Group 2, ST-gelatin (30 wt%) and non-treated anti-HGF antibody (0.2 wt%); or Group 3, ST-gelatin (30 wt%) and anti-HGF ST-Ab (0.2 wt%)], as shown in Fig. 6A. As shown in Fig. 6B, without the gel layer system (control: Group 0) and with the simple ST-gelatin gel layer system (Group 1), the numbers of invaded cells markedly increased with the addition of HGF, regardless of HGF concentration. There was negligible difference in the number of invaded cells between these two groups at respective HGF concentration. On the other hand, the numbers of invaded cells in Groups 2 and 3 were suppressed in spite of the addition of HGF and a markedly suppressive effect on invasion was noted especially at a low concentration (10 ng/ml). These findings indicate that HGF is neutralized by anti-HGF antibody in the gel regardless of free non-treated anti-HGF antibody or fixed anti-HGF ST-Ab.

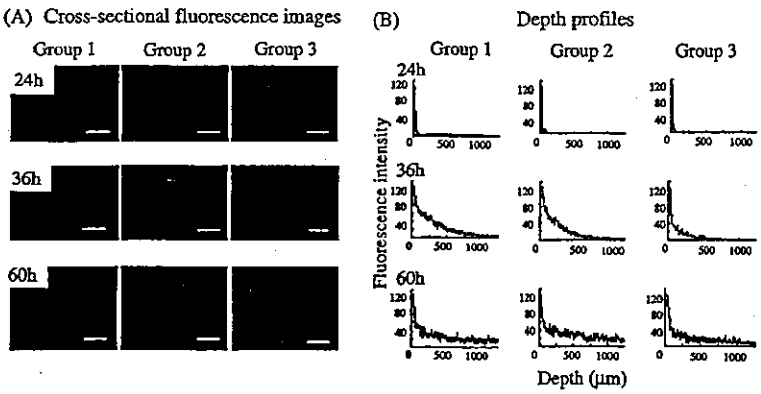

Fig. 5. The permeation of rhodamine-conjugated BSA into three different gels [Group 1, ST-gelatin (30 wt%); Group 2, ST-gelatin (30 wt%) and non-treated anti-BSA antibody (0.2 wt%); or Group 3, ST-gelatin (30 wt%) and anti-BSA ST-Ab (0.2 wt%)] was observed by a CLSM. (A) Cross-sectional fluorescence images. Bar: 500 μm. (B) Depth profiles (fluorescence intensity as a function of the distance from the gel surface).

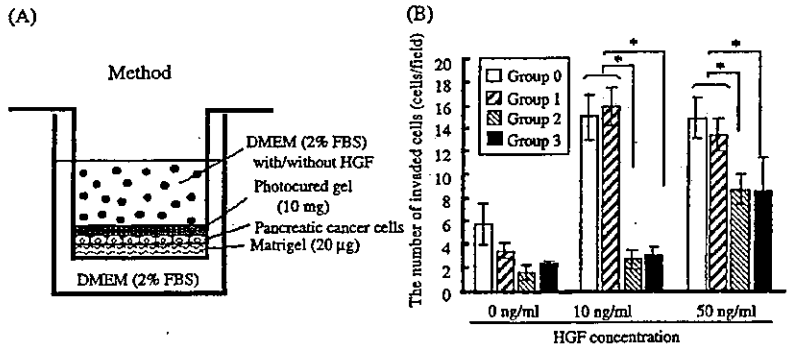

Fig. 6. Invasion assay was performed with modifications using 10 mg each of the three kinds of photocured gelatin gels [Group 1, ST-gelatin (30 wt%) only; Group 2, ST-gelatin (30 wt%) and non-treated anti-human HGF antibody (0.2 wt%); or Group 3, ST-gelatin (30 wt%) and anti-human HGF ST-Ab (0.2 wt%)]. ($n = 3$) In the control group, a gel was not used. ($n = 3$) Statistical analysis was performed using analysis of variance (ANOVA). Post-hoc comparisons were made by the Scheffe analysis. Differences were considered significant at $p<0.05$. In Groups 0 and 1, the numbers of invaded SUIT-2 cells increased with the addition of HGF. On the other hand, in Groups 2 and 3, HGF-dependent invasion of SUIT-2 cells was significantly suppressed. $^{*}p<0.05$.

4. Discussion

We newly prepared ST-Ab with a minimal loss of its affinity to antigen, which was copolymerized with ST-gelatin to produce a tissue-adhesive co-gel of ST-gelatin and ST-Ab (Fig. 2A). Our previous studies showed that ST-gelatin can serve as an in situ formable and bioactive-substance-immobilizable matrix upon photopolymerization to produce a gel under visible-light irradiation, which adheres well on surgically resected tissues [26–28]. When a non-treated anti-BSA antibody was immobilized in the ST-gelatin gel, antibody was released from the gel, whereas a mixture of anti-BSA ST-Ab and ST-gelatin formed a copolymerized gel upon visible-light irradiation, from which ST-Ab was less released from the gel (Fig. 4). In addition, the depth profile analysis of the distribution of the dye-conjugated BSA as an antigen in the gel clearly showed limited or retarded permeation of antigen into the co-gel of ST-Ab and ST-gelatin at an early period (Fig. 5). These findings imply that the co-gel using ST-Ab works as an antigen-barrier, which prevents local antigen permeation into a target tissue coated with a gel.

In an in vitro invasion assay, the inhibitory potential for HGF-dependent invasion was observed in Groups 2 (ST-gelatin + non-treated anti-HGF antibody) and 3 (ST-gelatin + anti-HGF ST-Ab) at almost the same extent (Fig. 6B). The inhibitory effect was dose-dependent, and more profound at a low HGF concentration. Combined with the result of BSA permeation experiment determined by a CLSM, it is highly anticipated that a sufficiently large amount of antibody immobilized or chemically bound in a tissue-adhesive gel completely blocks HGF activity into resected tissues.

An antibody immobilization approach is beneficial in terms of ease in preparation of an immobilized gel (Fig. 1B), but its shortcoming is that antibodies may diffuse from a gel and transfer to distant site, resulting in gradual decrease of local concentration of antibody. On the other hand, an antibody-bound approach (Fig. 1C) does not have such a shortcoming because an antibody is fixed by polymerization in the gel.

The proposed strategy may be a promising cytostatic approach for cancer therapy, which minimizes migration and proliferation of remnant cancer cells as a cytokine-barrier. If needed, anti-EGF, anti-bFGF, anti-VEGF and anti-TGF-β antibodies could be styrenated in the same manner, and copolymerized with ST-gelatin to produce a co-gel. When a cytotoxic substance, such as an anti-cancer drug, was immobilized in a co-gel of ST-gelatin and anti-cytokine ST-Ab and continuously released from a co-gel to a target tissue (Fig. 1D) [28], its synergetic effect derived from combined cytostatic and cytotoxic approaches could bring in a powerful therapeutic outcome without serious systemic adverse effects.

5. Conclusions

ST-Ab newly prepared was copolymerized with ST-gelatin to produce a tissue-adhesive co-gel, which may act as antigen-barrier. When anti-cytokine antibody was fixed in a gel, the cytokine, produced in surgical procedure and accumulated in the peritoneal fluid, was captured by or complexed with its antibody in a gel, resulting in prevention of the permeation of the cytokine into the resected tissue. Such local antibody therapy may help inhibit malignant behavior of remnant cancer cells without retarded wound healing at distant sites.

Acknowledgements

This study is financially supported by Promotion Fundamental Studies in Health Science of the Organization for Pharmaceutical Safety and Research (OPSR, contract grant number: 97-15) and Grant-in-Aid for Scientific Research from Ministry of Education, Culture, Sports, Science, and Technology of Japan (contract grant number: A2-12358017 and B2-12470277). The authors wish to thank K. Yasutake for excellent technical assistance.

References

[1] Yapp DT, Lloyd DK, Zhu J, Lehnert SM. Cisplatin delivery by biodegradable polymer implant is superior to systemic delivery by osmotic pump or i.p. injection in tumor-bearing mice. Anticancer Drugs 1998;9:791–6.

[2] Tamura T, Fujita F, Tanimoto M, Koike M, Suzuki A, Fujita M, Horikiri Y, Sakamoto Y, Suzuki T, Yoshino H. Anti-tumor effect of intraperitoneal administration of cisplatin-loaded microspheres to human tumor xenografted nude mice. J Control Rel 2002;80: 295–307.

[3] St'astny M, Plocova D, Etrych T, Kovar M, Ulbrich K, Rihova B. HPMA-hydrogels containing cytostatic drugs. Kinetics of the drug release and in vivo efficacy. J Control Rel 2002;81: 101–11.

[4] Lee CM, Tanaka T, Murai T, Kondo M, Kimura J, Su W, Kitagawa T, Ito T, Matsuda H, Miyasaka M. Novel chondroitin sulfate-binding cationic liposomes loaded with cisplatin efficiently suppress the local growth and liver metastasis of tumor cells in vivo. Cancer Res 2002;62:4282–8.

[5] Cienfuegos JA, Manuel FA. Analysis of intraoperative radiotherapy for pancreatic carcinoma. Eur J Surg Oncol 2000;26:S13–5.

[6] Takeda S, Inoue S, Kaneko T, Harada A, Nakao A. The role of adjuvant therapy for pancreatic cancer. Hepatogastroenterology 2001;48:953–6.

[7] Sperti C, Pasquali C, Piccoli A, Pedrazzoli S. Recurrence after resection for ductal adenocarcinoma of the pancreas. World J Surg 1997;21:195–200.

[8] Hofer SO, Molema G, Hermens RA, Wanebo HJ, Reichner JS, Hoekstra HJ. The effect of surgical wounding on tumour development. Eur J Surg Oncol 1999;25:231–43.

[9] Di Renzo MF, Poulsom R, Olivero M, Comoglio PM, Lemoine NR. Expression of the Met/hepatocyte growth factor receptor in human pancreatic cancer. Cancer Res 1995;55:1129–38.

[10] Ebert M, Yokoyama M, Friess H, Buchler MW, Korc M. Coexpression of the c-met proto-oncogene and hepatocyte growth factor in human pancreatic cancer. Cancer Res 1994;54:5775–8.

[11] Jiang W, Hiscox S, Matsumoto K, Nakamura T. Hepatocyte growth factor/scatter factor, its molecular, cellular and clinical implications in cancer. Crit Rev Oncol Hematol 1999;29:209–48.

[12] Matsumoto K, Date K, Ohmichi H, Nakamura T. Hepatocyte growth factor in lung morphogenesis and tumor invasion: role as a mediator in epithelium-mesenchyme and tumor-stroma interactions. Cancer Chemother Pharmacol. 1996;38:S42–7.

[13] Date K, Matsumoto K, Kuba K, Shimura H, Tanaka M, Nakamura T. Inhibition of tumor growth and invasion by a four-kringle antagonist (HGF/NK4) for hepatocyte growth factor. Oncogene 1998;17:3045–54.

[14] Date K, Matsumoto K, Shimura H, Tanaka M, Nakamura T. HGF/NK4 is a specific antagonist for pleiotrophic actions of hepatocyte growth factor. FEBS Lett 1997;420:1–6.

[15] Kuba K, Matsumoto K, Ohnishi K, Shiratsuchi T, Tanaka M, Nakamura T. Kringle 1-4 of hepatocyte growth factor inhibits proliferation and migration of human microvascular endothelial cells. Biochem Biophys Res Commun 2000;279:846–52.

[16] Kuba K, Matsumoto K, Date K, Shimura H, Tanaka M, Nakamura T. HGF/NK4, a four-kringle antagonist of hepatocyte growth factor, is an angiogenesis inhibitor that suppresses tumor growth and metastasis in mice. Cancer Res 2000;60:6737–43.

[17] Maehara N, Matsumoto K, Kuba K, Mizumoto K, Tanaka M, Nakamura T. NK4, a four-kringle antagonist of HGF, inhibits spreading and invasion of human pancreatic cancer cells. Br J Cancer 2001;84:864–73.

[18] Kimura F, Miyazaki M, Suwa T, Kadoyama C, Itoh H, Ambiru S, Shimizu H, Nakagawa K. Correlation between human hepatocyte growth factor and interleukin-6 concentrations after surgery. Hepatogastroenterology 1999;46:1030–5.

[19] Kimura F, Miyazaki M, Suwa T, Kakizaki S, Itoh H, Kaiho T, Ambiru S, Shimizu H, Togawa A. Increased levels of human hepatocyte growth factor in serum and peritoneal fluid after partial hepatectomy. Am J Gastroenterol 1996;91:116–21.

[20] Miyata K, Taniguchi H, Tsubouchi H, Daikuhara Y, Takahashi T. Levels of human hepatocyte growth factor (hHGF) in peritoneal fluid after partial hepatectomy. Hepatogastroenterology 1996;43:1594–600.

[21] von Schweinitz D, Faundez A, Teichmann B, Birnbaum T, Koch A, Hecker H, Gluer S, Fuchs J, Pietsch T. Hepatocyte growth-factor-scatter factor can stimulate post-operative tumor-cell proliferation in childhood hepatoblastoma. Int J Cancer 2000;85:151–9.

[22] Zagury D, Le Buanec H, Bizzini B, Burny A, Lewis G, Gallo RC. Active versus passive anti-cytokine antibody therapy against cytokine-associated chronic diseases. Cytokine Growth Factor Rev 2003;14:123–37.

[23] Gordon MS, Margolin K, Talpaz M, Sledge Jr GW, Holmgren E, Benjamin R, Stalter S, Shak S, Adelman D. Phase I safety and pharmacokinetic study of recombinant human anti-vascular endothelial growth factor in patients with advanced cancer. J Clin Oncol 2001;19:843–50.

[24] Ferrara N. Role of vascular endothelial growth factor in physiologic and pathologic angiogenesis: therapeutic implications. Semin Oncol 2002;29:S10–4.

[25] Herbst RS, Shin DM. Monoclonal antibodies to target epidermal growth factor receptor-positive tumors: a new paradigm for cancer therapy. Cancer 2002;94:1593–611.

[26] Okino H, Nakayama Y, Tanaka M, Matsuda T. In situ hydrogelation of photocurable gelatin and drug release. J Biomed Mater Res 2002;59:233–45.

[27] Okino H, Manabe T, Tanaka M, Matsuda T. Novel therapeutic strategy for prevention of malignant tumor recurrence after surgery: local delivery and prolonged release of adenovirus immobilized in photocured, tissue-adhesive gelatinous matrix. J Biomed Mater Res 2003;66:643–51.

[28] Okino H, Maeyama R, Manabe T, Matsuda T, Tanaka M. Transtissue, sustained-release of gemcitabine from photocured gelatin gel inhibits the growth of heterotopic human pancreatic tumor in nude mice. Clin Cancer Res 2003;9:5768–93.

[29] Matsuda T, Magoshi T. Preparation of vinylated polysaccharides and photofabrication of tubular scaffolds as potential use in tissue engineering. Biomacromolecules 2002;3:942–50.

[30] Iwamura T, Katsuki T, Ide K. Establishment and characterization of a human pancreatic cancer cell line (SUIT-2) producing carcinoembryonic antigen and carbohydrate antigen 19-9. Jpn J Cancer Res 1987;78:54–62.

Available online at www.sciencedirect.com
SCIENCE DIRECT®
Biomaterials 26 (2005) 1675–1684
Biomaterials
www.elsevier.com/locate/biomaterials

Photo-polymerized microarchitectural constructs prepared by microstereolithography (μSL) using liquid acrylate-end-capped trimethylene carbonate-based prepolymers

Il Keun Kwon, Takehisa Matsuda*

Division of Biomedical Engineering, Graduate School of Medicine, Kyushu University, 3-1-1 Maidashi, Higashi-ku, Fukuoka 812-8582, Japan

Received 2 April 2004; accepted 25 June 2004
Available online 20 August 2004

Abstract

Precision microarchitectural constructs made of acrylated trimethylene carbonate (TMC)-based liquid prepolymers were photo-polymerized using a custom-designed microstereolithographic apparatus. In this study, three different photo-polymerizable liquid prepolymers were prepared by the polymerization of TMC with a low molecular weight poly(ethylene glycol) (PEG) (mol. wt. 200 or 1000); designated as PEG200 or PEG1000, respectively or trimethylolpropane (TMP) as an initiator, and subsequently end-capped with an acrylate group. As a result of layer-by-layer photo-irradiation of the prepolymer with a movable ultraviolet light pen driven by computer-aided design, a three-dimensional (3D) micropillar array, a microbank array, a microcone array, and multi-microtunnels formed on a platform plate or a glass plate were precisely fabricated. The PEG-based polymers exhibited a very low cell adhesion potential, whereas the TMP-based hydrophobic polymer exhibited high cell adhesion and proliferation potentials. The microbank array, which consisted of a plate made of the TMP-based polymer and microbanks made of the PEG200-based polymer, caused cell adhesion and proliferation only on the plate. Upon the implantation of microcone arrays under the subcutis of rats, the photo-polymerized construct made of the poorly swellable PEG200-based polymer exhibited only surface erosion and limited drug loading and releasing potentials. On the other hand, the photo-polymerized construct made of the highly swellable PEG1000-based polymer exhibited not only surface erosion but also bulk erosion and high drug loading and releasing potentials. In this paper, we discuss their potential biomedical applications.

Keywords: Microstereolithography (μSL); Acrylated liquid prepolymer; Photo-polymerization; Microarchitectures; Degradation; Drug release

1. Introduction

Stereolithography (SL), a rapid photo-typing technique, allows the integral formation of three-dimensional (3D) constructs layer-by-layer photo-polymerization using computer-aided design (CAD)/computer-aided manufacturing (CAM) with an ultraviolet (UV) light pen and a photo-polymerizable liquid prepolymer [1–4]. Microstereolithographic (μSL) allows a precision macroshaping and microarchitecturing of a device or scaffold design, and surface architecture for advanced medical procedures [5–10].

To this end, the authors have been developing photo-polymerizable biodegradable liquid prepolymers and their photo-polymerization processes. Our previous studies showed that prepolymers, composed of ε-caprolactone (CL) and trimethylene carbonate (TMC), end-capped with photo-reactive groups, such as coumarin [11–14], phenylazide [15], or acrylate [16], are rapidly converted from liquid to solid upon photo-irradiation. Furthermore, μSL microarchitectures, such as microneedles, microcylinders, microbanks, and microlattices on a platform, were feasible using di-acrylated poly(CL/TMC) with a custom-designed μSL

*Corresponding author. Tel.: +81-92-642-6210, fax: +81-92-642-6212.
E-mail address: matsuda@med.kyushu-u.ac.jp (T. Matsuda).

0142-9612/$ - see front matter © 2004 Elsevier Ltd. All rights reserved.
doi:10.1016/j.biomaterials.2004.06.041

apparatus [17]. As an extension of a series of photo-polymerizable biodegradable liquid prepolymers, we very recently synthesized a series of acrylated biodegradable liquid TMC-based prepolymers, which were obtained by the polymerization of TMC with a low molecular weight PEG (mol. wt. 200 or 1000) or trimethylolpropane (TMP) as an initiator, and subsequently acrylate end-capped. The hydrolytical surface erosion of completely photo-polymerized films by visible-light irradiation in the presence of camphorquinone was thoroughly evaluated by a force-indentation technique using atomic force microscopy (AFM) [18]. The photo-polymerized films prepared from prepolymers with a low molecular weight PEG (PEG200) and TMP exhibited a much lower hydrolysis potential than polymers prepared from PEG1000-derived prepolymers in terms of weight loss, water uptake and swellability [18].

In this study, as an extension of our series of studies on μSL, various microarchitectures using three different TMC-based liquid prepolymers, previously prepared by us, were photo-polymerized using the custom-designed μSL system for prototype models, which can be translated to real tissue engineering scaffolds. As an application, photo-polymerized microarchitectural constructs (microarrays) consisted of a cell-adhesive plate and noncell-adhesive banks that were prepared for regiospecific 2D cell culture. For the 3D culture system, multi-microtunnel constructs were photo-polymerized. A multi-needle microarchitecture was photo-polymerized as a prototype model of sustained release of a drug in the deep region of a diseased tissue. The in vivo hydrolytic degradation behavior of photo-polymerized microcone constructs made of PEG-based polymers, and their drug loading and in vivo releasing potentials under the subcutis of rats were demonstrated (Fig. 1).

(A) **Acrylated prepolymer (TMC/PEG200)**

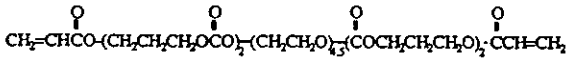

(B) **Acrylated prepolymer (TMC/PEG1k)**

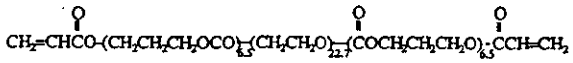

(C) **Acrylated prepolymer (TMC/TMP)**

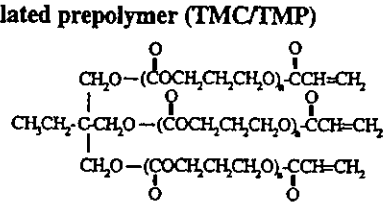

Fig. 1. Chemical structures of photo-polymerizable TMC-based liquid prepolymers derived from (A) PEG200, (B) PEG1000, and (C) TMP.

2. Materials and methods

2.1. General procedure

All solvents and reagents were purchased from either Wako Pure Chemical Industries, Ltd. (Osaka, Japan) or Sigma-Aldrich Japan, Inc. (Tokyo, Japan). TMC was prepared according to the method described in our previous paper and recrystallized from a mixed solvent of ethyl acetate and hexane [11]. TMP was recrystallized from acetone. PEG [mol. wt. of 200 or 1000, according to the manufacturer's information (Wako)] was purified by precipitation from cold hexane and subsequently vacuum-dried prior to use. Acryloyl chloride was used as obtained without further purification. Other solvents and reagents were purified by distillation. ^{1}H-NMR spectra were recorded on a JNM-AL300 system (JEOL, Tokyo, Japan). Chemical shifts are given in δ values from Me_4Si as an internal standard. The number-average molecular weight (M_n) of each prepolymer was determined by gel permeation chromatography (GPC), which was carried out on a high-performance liquid chromatograph (HPLC, JASCO-JMBS, Tokyo, Japan) equipped with a TSK-GEL column α-3000 (TOSOH, Tokyo, Japan) using PEG as a standard and tetrahydrofuran (THF) as an eluent. Viscosity of each prepolymer was determined by a cone-and-plate viscometer (TV-20, Tokisangyo Co. Ltd., Tokyo, Japan) with a rotational cone rotor (1°34′ × R24) under a shearing rate (1 rpm), a torque (5750 μN m) at 25 °C, and expressed as Pa s. UV irradiation was carried out using a 250-W mercury–xenon (Hg–Xe) lamp (Hamamatsu Photonics L5662-02, Shizuoka, Japan). The intensity of UV light was measured at 365 nm on TOPCON UVR-25 (Tokyo, Japan).

2.2. Synthesis of acrylate-end-capped prepolymer

A typical procedure for the preparation was as follows [18]. TMC-based oligomers were prepared using TMC as the monomer and PEG (mol. wt. 200 or 1000) or TMP as an initiator and tin(II)2-ethylhexanoate as a catalyst (feed molar ratios are shown in Table 1). The reaction was carried out for 4 h at 200 °C, followed by heating for 2 h at 160 °C in a flask in N_2 atmosphere. The resultant oligomer was dissolved in dichloromethane. Subsequently, an excess of acryloyl chloride was added to this flask in N_2 atmosphere and the reaction mixture was stirred for 8 h at 50 °C. The prepolymer was precipitated from excess hexane and vacuum-dried at 30 °C. The resultant prepolymer was viscous liquid at room temperature. Acrylate content was determined from peak intensities in the ^{1}H-NMR spectra relative to those of the vinyl group and PEG or TMP unit yielding the following results: ^{1}H-NMR (300 MHz, $CDCl_3$, ppm): $\delta = 2.05$ (multiplet), 3.65

Table 1
Acrylate-endcapped liquid TMC-based prepolymers

Prepolymer code	Initiator	Initial feed (molar ratio)	Acrylate end-capped prepolymer				Photo-polymerized film[a]	
			Composition[b]	Degree of acrylation[b] (%)	M_n[c]	Viscosity[d] (Pa s)	Receding contact angle[e]	DW[f]
		TMC: Iniator	TMC: Iniator					
T/P200	PEG200	1:0.250	1:0.250	90	8.0×10^2	1.3 ± 0.05	27 ± 3.56	2
T/P1k	PEG1000	1:0.076	1:0.076	97	2.4×10^3	2.1 ± 0.33	<5.0	30
T/TMP	$CH_3CH_2C(CH_2OH)_3$	1:0.167	1:0.167	92	1.1×10^3	2.6 ± 0.22	47.4 ± 5.33	1

[a]Photo-polymerizing conditions: liquid film of acrylated prepolymers (thickness; 0.2 mm). Photoirradiation at the intensity of 2 W/cm^2 at 365 nm for 1 min at room temperature.
[b]Molar ratio; determined by ^{1}H-NMR.
[c]Determined by GPC in THF (PEG standard). Mn: number-average molecular weight.
[d]Determined by a cone-plate viscometer using a rotational cone rotor (1° 34′ × R24): a shearing rate, 1 rpm; a torque, 5750 μN m, 25 °C ($n = 4$).
[e]Water contact angle measured by the sessile drop method ($n = 4$).
[f]The degree of water adsorptivity of photo-polymerized film after 2-day immersion in aqueous solution (see Eq. (1)).

(doublet), 4.24 (multiplet), 5.85 (doublet), 6.12 (quartet) and 6.42 (doublet).

2.3. UV-induced photo-polymerizing characteristics

Round liquid films (ϕ 10 mm) of the acrylated prepolymers were irradiated with the Hg–Xe lamp at a 2 W/cm^2. After the immersion of photo-polymerized films into excess dichloromethane to remove the soluble fraction, the insoluble polymers were dried and weighed. The gel content of the network was defined as the weight percentage of the insoluble part (W_g) with respect to that of the initial prepolymer (W): $W_g/W \times 100$.

2.4. Water contact angle

The surface wettability of photo-polymerized films was evaluated by measuring static contact angles toward deionized water using the sessile drop method with a contact angle meter (CA-D, Kyowa Interface Co. Ltd., Tokyo, Japan) at 25 °C.

2.5. Water adsorptivity

The photo-polymerized films were immersed for 2 days in an aqueous solution at 25 °C. The weight of swollen films (W_S) and that of dried films (W_D) were measured after wiping the surface with paper and vacuum drying, respectively. The degree of water adsorptivity (DW) was evaluated as

$$DW(\%) = 100 \times [W_S - W_D]/W_D. \quad (1)$$

2.6. Photo-polymerization using a μSL apparatus

A layer-by-layer photo-polymerization of microarchitectural constructs using a custom-designed μSL apparatus prepared in our previous study was carried out (Fig. 2) [17]. The μSL apparatus consisted of a movable light pen with a photo-mask (diameter, 50 μm), an optical fiber connecting the light pen and the light source (Hg–Xe lamp), a vertical elevator and controller (Sigma Koki MARK-41, Tokyo, Japan) driven by computer-assisted design, and a liquid prepolymer bath. The stage controller manipulated the movement of the light pen at a rate of 5 μm/s and photo-irradiation intensity was set at 2 W/cm^2 (365 nm wavelength), and the photo-polymerizable liquid prepolymer was refilled on the surface by lowering the vertical elevator table into the liquid prepolymer bath (200 μm/cycle). After completing all the steps, the resulting photo-polymerized construct was thoroughly washed with acetone and vacuum-dried.

2.7. Microscopy observations

A photo-polymerized construct was observed under a scanning electron microscope (SEM, JSM-840A, JEOL Ltd., Tokyo, Japan) after sputter coating with gold. The histological analysis of the subcutis of a rat was carried out under a light microscope (Olympus VANOX-S AHBS, Tokyo, Japan).

2.8. Cell culture examination

A photo-polymerized construct or film was sterilized with 70% ethanol, washed with PBS, air-dried, and placed at the bottom of a 24-well culture dish (Corning, NY). Fibroblasts (Swiss3T3, obtained from American Type Culture Collection, 5×10^4 cells/well) were seeded into the dish with Dulbecco's modified Eagle's medium (DMEM, Life Technologies Inc., Rockville, MD) supplemented with 10% fetal bovine serum (FBS, Life Technologies). The cells were maintained at 37 °C in a

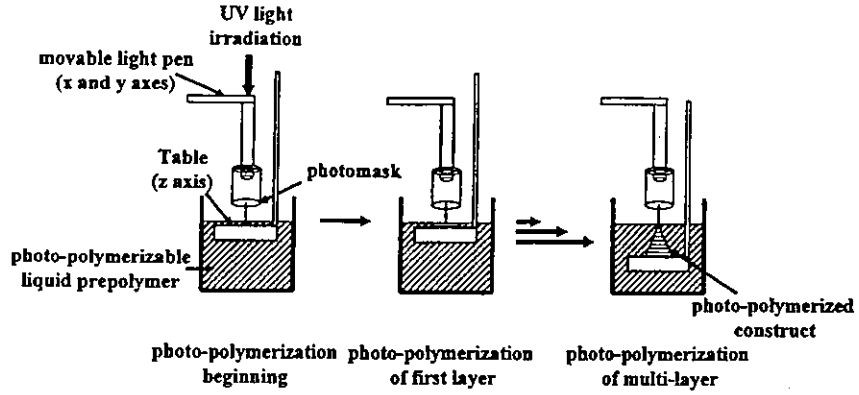

Fig. 2. Scheme of layer-by-layer photo-polymerization using a custom-designed microstereolithographic (μSL) rapid photo-typing apparatus.

humidified 5% CO_2 atmosphere. The cell number on the film was determined by NIH Image Software, and observation was carried out under a phase-contrast microscope (TE300, Nikon, Tokyo, Japan) after a certain incubation period.

2.9. *In vivo hydrolytic degradation behavior*

The photo-polymerized microcone array made of P(T/P200) or P(T/P1k) was washed with ethanol and vacuum-dried, then was implanted under the dorsal subcutis of a female Wister rat (about 400 g in weight). After 1- or 4-week implantation, the rat was dissected to remove the construct from the subcutis.

2.10. *Preparation of drug-loaded photo-polymerized constructs and implantation*

The microcone array, a photo-polymerized micro-architectural construct made of P(T/P200) or P(T/P1k), was immersed in 10 wt% dexamethasone (Sigma) aqueous solution for 2 days, washed with ethanol and vacuum-dried. The drug-loaded construct was implanted under the dorsal subcutis of a female Wister rat. After 1-week implantation, the rat was dissected to remove the surrounding tissue of the construct. The tissue was fixed in 1% aqueous formaldehyde solution (pH 7.4) for 12 h, and stained with hematoxylin eosin (HE).

3. Results

3.1. *Preparation of liquid acrylated TMC-based prepolymers and photo-polymerizing characteristics*

A series of liquid acrylated TMC-based prepolymers were prepared using a triol (TMP) or linear PEG with a molecular weight of 200 or 1000 [prepolymer codes were given as T/P200, T/P1k and T/TMP and their photo-polymerized films or constructs were designated as P(T/P200), P(T/P1k) and P(T/TMP), respectively, where T denotes TMC, and P200 and P1k denote PEG with molecular weights of 200 and 1000, respectively]. The TMP-based prepolymer is a trifunctional acrylated prepolymer, and the PEG-based prepolymers are bifunctional acrylated prepolymers. Table 1 summarizes the prepolymer compositions, degrees of acrylation, the molecular weights, and the viscosities of prepolymers. The resultant prepolymers (90–98% acrylation determined by ^{1}H-NMR spectroscopy) were viscous liquids. Viscosities of the prepolymers determined by a cone-and-plate viscometer ranged approximately 1.3–2.6 Pa s. The number-average molecular weights of the prepolymers, T/P200, T/P1k, and T/TMP, determined by GPC, were approximately 8×10^2, 2.4×10^3, and 1.1×10^3, respectively. The dependence of gel content of the network on UV-irradiation time for three acrylated prepolymers is shown in Fig. 3. Irrespective of the type of prepolymer, similar irradiation time-dependent photo-polymerizing characteristics of the prepolymers were observed: more than 95% of yield was achieved

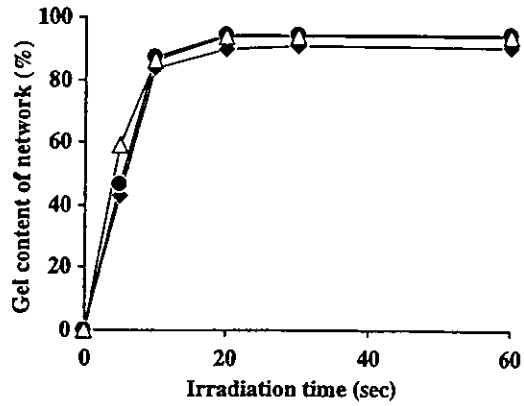

Fig. 3. UV-induced gel content of the network of TMC-based liquid prepolymers at an irradiation of 2 W/cm^2. Film thickness: 0.2 mm P(T/P200) (●), P(T/P1k) (♦), and P(T/TMP) (△).

within 20 s of photo-irradiation. Regarding the water contact angles of completely photo-polymerized films, PEG-based films exhibited low receding angles [27° for P(T/P200) and less than 5° for P(T/P1k)], whereas P(T/TMP) exhibited a relatively high receding angle (47.4°) (Table 1). Following the immersion of photo-polymerized films (photo-irradiation time; 1 min, photo-intensity; 2 W/cm^2) in water for 2 days, degree of water adsorptivity (DW) defined as Eq. (1) was as follows: approximately 30% for P(T/P1k), 2% for P(T/P200) and 1% for P(T/TMP) (Table 1).

3.2. Microstereolithographically (μsl) photo-polymerized constructs

Fig. 4 shows the design configurations of four different microarchitectural constructs (micropillar array, microcone array, microbank array on a platform plate, and multi-microtunnels on a glass plate). After the platform plates were prepared using a prepolymer, various microarchitectures were fabricated by layer-by-layer photo-polymerization using the same prepolymer used for platform plates except for multi-microtunnels. Before microarchitectural constructs were photo-polymerized, a platform plate, on which a construct was formed, was prepared by two cycles of parallel UV scanning (size, 5 mm × 5 mm; height, 400 μm) (Figs. 4A–C). Fig. 5A shows the micropillar array in which pillars (approximately 400 μm in diameter and 1200 μm in height) were formed on the platform plate, which was prepared by eight cycles of programmed scanning. Fig. 5B shows the microcone array (bottom diameter of cone, 650 μm; top diameter, 100 μm; height, 1800 μm) formed on the platform plate, which was photo-polymerized by gradually decreasing the diameter of the movable light pen from 500 to 0 μm (number of cycles of programmed scanning: 11). Fig. 5C shows the microbank array (width of bank, 300 μm; length, 5 mm; height, 1200 μm) formed on the platform plate (number of cycles: 8). Multi-microtunnels were prepared according to the configuration (Fig. 4D) on the glass plate at different cycles of layer photo-polymerization, and then stood up the constructs (see Fig. 6). The resultant constructs were easily removed from the glass plate.

Fig. 6 shows two types of multi-microtunnels; The first multi-microtunnel contains nine microtunnels

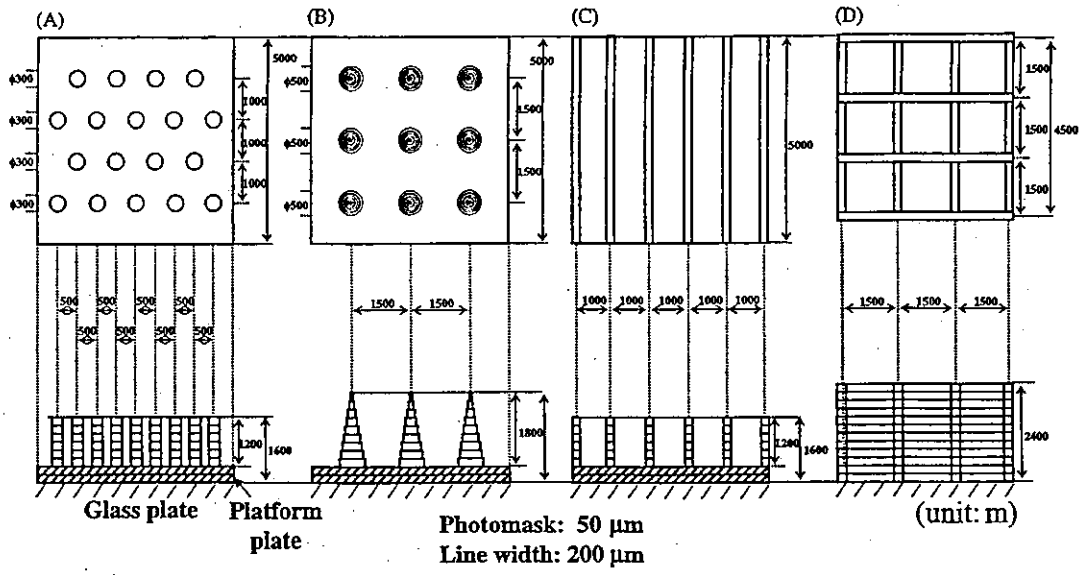

Fig. 4. Design configurations of microarchitectured constructs. Upper panels: top views; lower panel: cross-sectional views. (A) Micropillar array; (B) microcone array; (C) microbank array; and (D) multi-microtunnels.

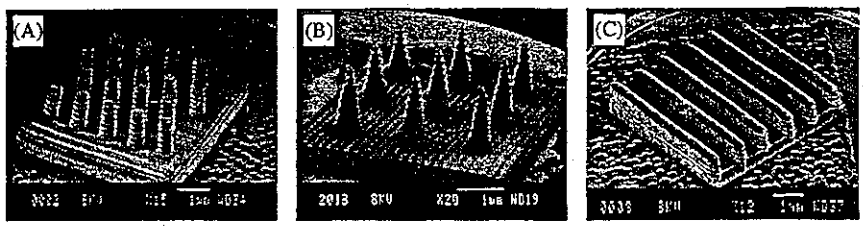

Fig. 5. SEM images of (A) micropillar array, (B) microcone array, and (C) microbank array prepared from the P(T/P200).

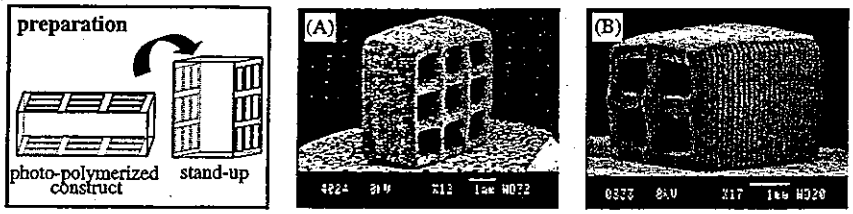

Fig. 6. SEM images of multi-microtunnels prepared from P(T/P200), (A) nine tunnels and (B) four tunnels.

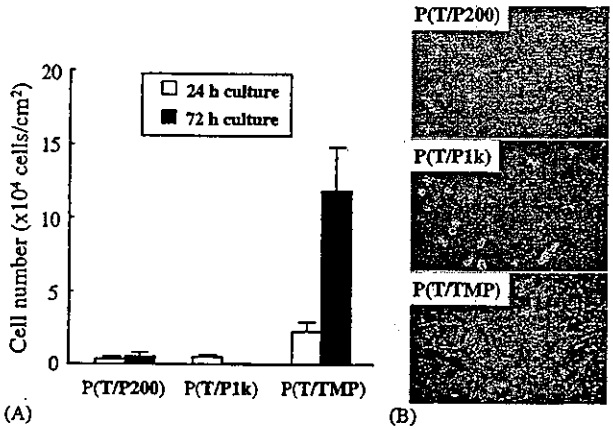

Fig. 7. Cell adhesion potential on three different photo-polymerized films: (A) cell number and (B) microscopy observation of the photo-polymerized films at 72 h culture.

(Fig. 6A). Each of the nine square microtunnels has a height and width of 800 μm and a tunnel length of 2400 μm (number of cycles: 12). Fig. 6B depicts four square microtunnels, each with a height and width of approximately 800 μm, and a tunnel length of 5000 μm (number of cycles: 25).

3.3. Cell adhesion potentials of photo-polymerized films

To determine the cell adhesion potential of photo-polymerized films, fibroblasts were seeded and cultured for up to 72 h. Both PEG-based films, P(T/P200) and P(T/P1k), exhibited a very low cell adhesion potential; concomitantly, markedly reduced spread and proliferation were observed. On the other hand, the relatively hydrophobic film (P(T/TMP)) exhibited a high cell adhesion and proliferation potentials as shown in Fig. 7.

3.4. Multi-microwells and composite microbank array for cell culture

Fig. 8 shows the multi-microwells prepared by photo-polymerization of noncell-adhesive P(T/P200) formed on the glass surface. Square wells were prepared by the photo-polymerization of cross-hatched banks (each well has the following dimensions: 800 μm × 800 μm, height of bank: about 200 μm) using a movable light pen for each 1 mm of square well (number of cycles: 1). When fibroblasts were seeded and cultured for 3 days on the multi-microwells, cells adhered and proliferated in the glass surface of wells, but little cell adhesion was observed on the banks. Fig. 9 shows the composite microbank array, which consisted of the plate with cell adhesive P(T/TMP) and microbanks with noncell-adhesive P(T/P200). Regarding the composite constructs, after completing the process using one liquid prepolymer, the construct, which was fixed on a *z*-axis movable table, was thoroughly washed with acetone and another liquid prepolymer bath was set at the depth of about 200 μm for the next photo-polymerization. Cells did not adhere to the banks, but cells well adhered and spread on the plate.

3.5. In vivo hydrolytic degradation behavior

Microcone arrays made of P(T/P200) and P(T/P1k) were implanted under the dorsal subcutis of a rat for 1 and 4 weeks. Fig. 10 shows the SEM images before and after the implantation. Some of the microcones in an array made of poorly swellable P(T/P200) were broken, probably due to tissue friction during implantation, and the crack size on the surface was slightly higher in 4-week implantation period (Figs. 10A, C, and E). On the other hand, for the microcone array made of highly swellable P(T/P1k), neither fracture nor cracks were observed for the swollen microarrays when harvested from tissues. However, SEM images showed large cracks, which were apparently created due to shrinkage during vacuum drying procedure for SEM sample preparation. The degree of crack formation at 4-week implantation appeared to be larger than that at 1-week implantation, suggesting that the degradation of P(T/P1k)-based photo-polymerized construct occurred not only on the surface but also in the bulk (Figs. 10B, D, and F).

3.6. Implantation of drug-loaded photo-polymerized constructs

An anti-inflammatory water-soluble drug (dexamethasone) in an aqueous solution was applied to two microcone arrays with different swelling properties;